Research **Open Access**

A technique for measuring spatial distribution of electromagnetic fields created by radio-frequency coils in MRI scanners

Alex Protopopov

Correspondence: proto.alex@hotmail.com

CrossMark
← Click for updates

Moscow Institute of Physics and Technology (MIPT), Russia Federal Scientific and Clinical Centre for Pediatric Hematology, Oncology, and Immunology (FSCC), Moscow, Russia.

Abstract

Non-uniformity of electromagnetic fields created by excitation coils in MRI scanners is an important factor, which must be measured and characterized in order to deliver adequate images and comply with safety regulations. This issue gradually becomes more and more important with commissioning of ever more powerful magnets and, consequently, higher radio frequencies with higher absorption rate in human body. With technological advance in thermal imaging, traditional measurement techniques based on discrete thermal sensors may soon be superseded by non-invasive optical methods, offering far greater flexibility and precision. The article introduces new technique of measuring spatial distribution of superficial electromagnetic field created by radio-frequency (RF) coils. The experiments described in this paper were performed using a General Electric 1.5 Tesla MRI scanner. Thermal images were acquired using a Testo 875 thermal camera, with a spatial resolution of 3 mm at a distance of 1 m, temperature range of 0-280°C, and sensitivity of 80 mK at 30°C. Solid-state phantoms of the size $700 \times 300 \times 5$ mm^3 were made from polymethylmethacrylate and shock-resistant polystyrene-dielectric low thermal conductivity materials opaque in infrared. The new method of measuring non-uniformity of fields created by RF coils is based on long-term stability of thermal map imprinted into plastic during scanning, proportionality of RF intensity to temperature variations, absence of optical artifacts due to opacity of phantoms, and subsequent numerical analysis of the entire digital map of temperature over the 700×300 mm^2 area of phantoms. The new method may prove feasible, convenient, accurate, inexpensive, and handy. The acquired thermal maps were converted into digital maps and analyzed numerically, computing principal statistical parameters such as peak-to-peak variation, real mean square, average, and most probable values.

Keywords: Magnetic resonance imaging, phantoms, coils, thermal imaging

Introduction

Spatial uniformity of radio-frequency (RF) fields created by coils in MRI scanners is an important factor, determining not only quality of images but also safety of patients. The stronger the intensity of RF field the bigger the amount of heat absorbed by human body. In every local point, this heat is proportional to intensity of RF field and specific absorption coefficient of the body in this particular point. Specific absorption rate (SAR) in human body is one of the most strictly regulated safety consideration that must not exceed certain values. Reported values of SAR are usually an average over the entire body. Sometimes, local (spot) values of SAR may significantly exceed the average value, causing thermal injury [1]. Therefore, spatial distribution of RF intensity must be known as an important safety consideration. Commonly, volumetric distribution of RF intensity is computed by simulation programs. Although state-of-the-art algorithms produce mostly reliable results [2], experimental validation is always necessary [3].

The most direct approach to measure volumetric distribution of RF intensity without creating disturbance to electromagnetic field is measuring tiny increases of temperature in weakly absorbing uniform dielectric medium. This technique, actually, associates spatial distribution of temperature with spatial distribution of RF intensity. The result gives correct representation of RF distribution because the absorbed heat is proportional to RF intensity, and the temperature variation

is proportional to the absorbed heat. There are two basic technologies for measuring temperature: invasive sensors, like optical fibers [4], and infrared (IR) imaging [5]. Both have their pro and cons. Sensors inevitably disturb original electromagnetic fields and, consequently, temperature fields. However, they provide data from inner parts of a phantom. On the contrary, imaging techniques are ambiguous about volumetric temperature fields because the result is integrated over the line-of-sight trajectory of light, but on the other hand, they do not disturb electromagnetic field and provide incomparably better spatial resolution than can be attained by only few sensors. The present paper introduces experimental technique that avoids volumetric ambiguity. With this improvement, the IR imaging may be considered as the technology of choice.

Materials and methods

Experiments were performed at a 1.5 Tesla General Electric MRI scanner. Thermal maps were acquired using a Testo 875 thermal camera, with a spatial resolution of 3 mm at a distance of 1 m, a temperature range of 0-280ºC, and a sensitivity of 80 mK at 30ºC.

Design of phantoms

Designing phantoms for IR imaging, two basic considerations should be taken into account. Firstly, commonly used liquid-filled phantoms may deliver incorrect measurements as the liquid stirs up due to thermal convection and vibrations, thus disturbing original distribution. Secondly, walls of the container may be opaque in IR domain, blocking IR radiation from the simulating liquid itself. Then, the IR camera shows not the exact temperature distribution but instead temperature distribution on the surface of the wall. Thirdly, even if the walls are made IR transparent, the signal measured by the IR camera is the integral over the line-of-sight trajectory of light, requiring either complicated mathematical compensation or very rough assumptions about uniformity in order to extract quantitative results. On the contrary, in the technique proposed in this paper, thin sheets of solid plastic substantially opaque in IR are used. Solidity of the phantom ensures stability of the temperature map through several minutes-time sufficient to take the phantom out of the scanner and make IR images, whatever its position was-horizontal or vertical. Opacity in IR domain guarantees that only surface temperature is recorded, making the measurement mathematically unambiguous. High electro-dynamic quality of plastics like polymethylmethacrylate (PMMA) or shock-resistant polystyrene (SRPS or polystyrol) ensures absence of predominant surface absorption of radio-frequency (RF) energy (skin-effect), which means mainly bulk absorption and uniformity over almost negligible (5mm) thickness of the phantom. Finally, changing position of such a phantom in the direction normal to its plane, it is possible, in principle, to obtain 3D distribution of RF intensity. Considering IR imaging of liquid-filled phantoms, it should be remembered

that only axial (parallel to B_0) views are available because the IR camera cannot be placed inside the scanner. With solid phantoms, all directions of observation are available as the phantom can be positioned and rotated as necessary inside the scanner and extracted after exposure without disturbance to temperature map imprinted in the phantom.

The only disadvantage of solid phantoms is that the material they use (plastic) may not normally simulate absorption of human body. It means that, from purely theoretical point of view, the RF coils are loaded to electromagnetic substance they were not designed for. As such, an objection may be put forward that plastic phantom disturbs pre-designed spatial distribution of the RF field. However, the scale of such a disturbance is expected to be of the order of the ratio of SAR to RF coil power. With SAR less than 20 W/kg and RF power about 20 kW, it means that disturbance of only 0.1% can be expected. Therefore, from practical point of view, this objection may be disregarded.

Mechanical strength and easy machining of PMMA and SRPS makes it possible to accurately make phantoms of exact predefined shape with the precision of less than 1 mm. **Figure 1** shows the shape of the phantoms that were used in experiments.
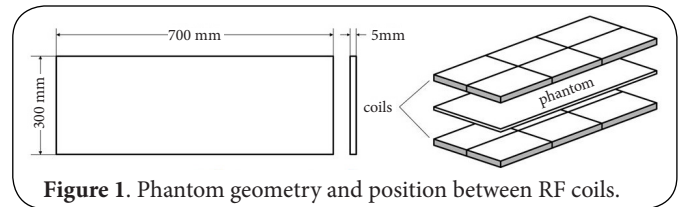

Figure 1. Phantom geometry and position between RF coils.

Characterization of phantoms

Opacity for IR radiation was tested according to **Figure 2**. Heated 40°C cup with water was placed behind the phantoms. Clearly, transparency of both PMMA and SRPS phantoms may be neglected.
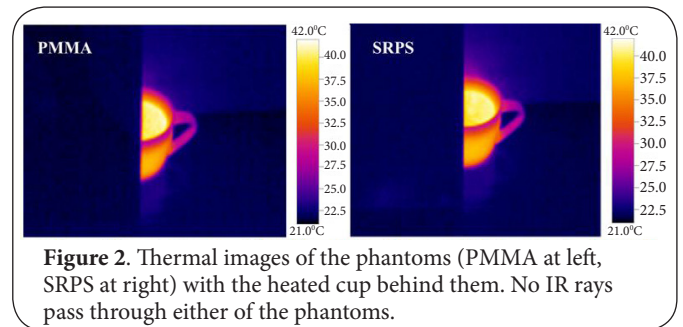

Figure 2. Thermal images of the phantoms (PMMA at left, SRPS at right) with the heated cup behind them. No IR rays pass through either of the phantoms.

Thermal conductivity of the phantom material must be small enough in order to prevent diffusion of heat from more to less heated areas, thus preserving the shape of a thermal map for several minutes needed to extract the phantom and make

measurements. **Figures 3** and **4** show how thermal distribution transforms in time in two consecutive moments 9 min one after another. Heated areas were formed by putting hot cup on the phantom surface.
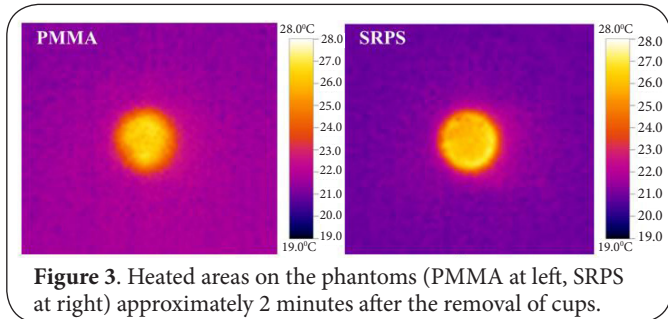
Figure 3. Heated areas on the phantoms (PMMA at left, SRPS at right) approximately 2 minutes after the removal of cups.
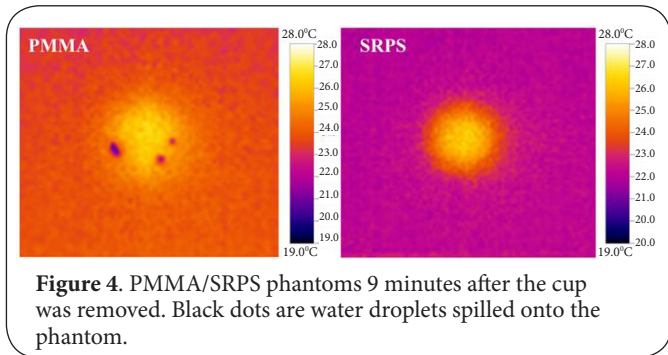
Figure 4. PMMA/SRPS phantoms 9 minutes after the cup was removed. Black dots are water droplets spilled onto the phantom.

Figure 5. Excitation coil. The ruler is placed for the scale.

Figure 6. Sequence No.1. Exposed phantoms clearly show regular structure of temperature, correlated with the coil geometry. The PMMA (at left) phantom is heated more efficiently than the SRPS one (at right).

From these results it follows that, during 2-3 minutes that are needed to extract the phantom from the scanner and capturer the IR image, spatial distribution of temperature does not change much. Only after several times longer interval sharpness of the borders dissolves, changing significantly initial distribution. Thus, acting quickly, reliable results can be obtained. **Figures 3** and **4** show that SRPS with thermal conductivity 0.1-0.14 W/(m×K) gives sharper image than PMMA with thermal conductivity 0.17-0.25 W/(m×K). Therefore, it may be recommended that the phantom material should have thermal conductivity less than 0.1 W/(m×K).
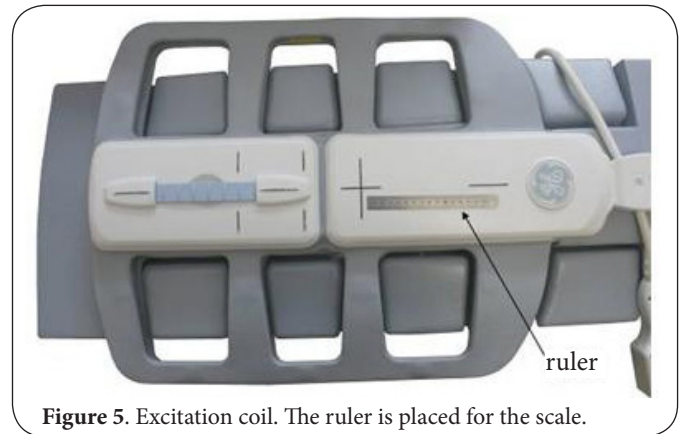
Results
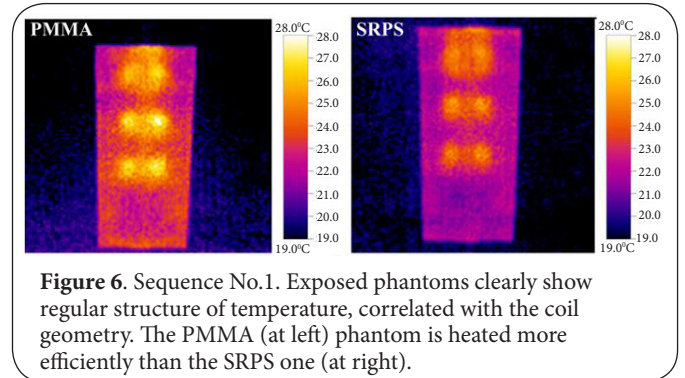### Experimental measurements
Experiments were performed at the following conditions. Excitation coil geometry is shown in **Figure 5**.

Figure 6 presents thermal pictures of the phantoms after exposure. Phantoms made of PMMA and SRPS were subjected to MRI scanning sequences. The first sequence was a T2 weighted frFSE sequence with TE=110 ms, TR=3280 ms, and the echo train of 21. It consisted of 12 slices and its duration was 2 minutes 30 seconds.

The second sequence was T1 weighted FSE sequence with TE=10 ms, TR=580 ms, and the echo train of 2. It consisted of 12 slices and its duration was 4 minutes 22 seconds.

A quick calculation shows, that the first sequence applied approximately 45 90-degree pulses, and 960 180-degree pulses, which, in terms of energy radiated, is equivalent to 1965 90-degree pulses applied over 2 minutes 30 seconds. On the other hand, the second sequence applied approximately 452 90-degree pulses and 903 180-degree pulses, which is equivalent to 2258 90-degree pulses applied over 4 minutes 22 seconds. This shows that the two sequences are quite similar in terms of total energy radiated, and the difference in phantom temperature comes mostly from the difference in sequence duration.

From the above results it follows that the RF coil shows regular spatial non-uniformity with definite maxima and minima, correlated with the coil's loop structure. In order to characterize these variations numerically, numerical analysis must be applied.

Numerical analysis
Thermal variations across the phantom, showing spatial distribution of RF intensity, can be converted into digital map, assuming linear functionality between the signal in each pixel of the IR image and the temperature. In turn, the IR image is the result of conversion of the sensor signal into temperature. Such conversion is a complicated and essentially nonlinear transformation, which includes many unknown parameters such as source irradiance, distance to the source,

Figure 7. Sequence No.2. Same structure and roughly the same heating.
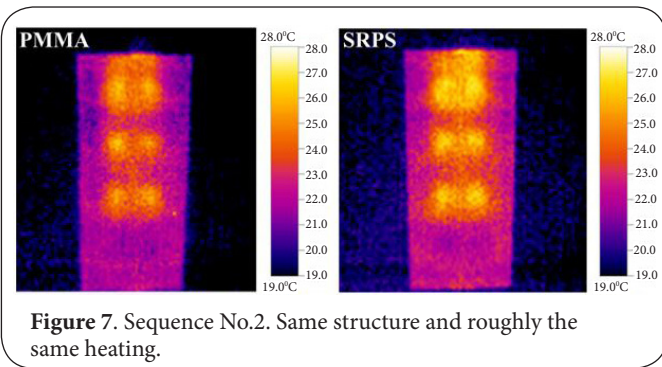
spectral sensitivity of the sensor, etc. Therefore, the values of temperature that the camera displays are not the exact temperatures but only factory-calibrated approximations. Manufacturers of IR cameras never disclose precision of those approximations in order not to compromise the product. Therefore, those users who want to be sure about the results have to make their own verification. The only parameter that is important for our application is linearity of the function that converts pixel amplitude into temperature. To verify that, we use the option of the grey-scale output. The luminance of the grey-scale picture is described by an 8-bit integer n, ranging from 0 to 256. The value 256 corresponds to the brightest pixel - white, and the value 0 corresponds to the darkest one - black. The grey-scale bar that the IR camera displays is always calibrated linearly and equidistantly in temperature (**Figure 8**). It means that there must be linear functionality between the vertical pixel number and the temperature. The question now stands as follows: is n a linear function of a vertical pixel? If it is, then the temperature is a simple linear function of n :

$$T = \alpha + \beta \cdot n \; ; \qquad (1)$$
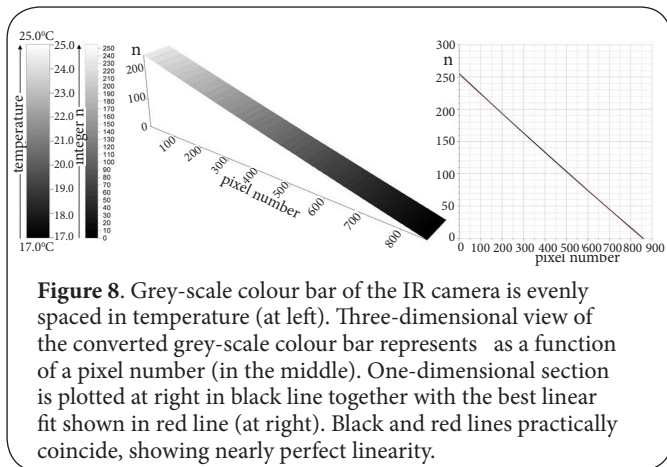
Figure 8. Grey-scale colour bar of the IR camera is evenly spaced in temperature (at left). Three-dimensional view of the converted grey-scale colour bar represents as a function of a pixel number (in the middle). One-dimensional section is plotted at right in black line together with the best linear fit shown in red line (at right). Black and red lines practically coincide, showing nearly perfect linearity.

and parameters α and β can be easily computed from $T_{\max}$ and $T_{\min}$ for any picture. If not, then our computations

may be not correct. Let us convert the gray-scale colour bar produced by the camera into digital array and analyze its linearity. **Figure 8** gives the answer.

Thus, conversion is nearly perfect, and we may trust the numerical computations below.

For the beginning, **Figure 9** presents three-dimensional (3D) portraits of the results shown in **Figures 6** and **7**.
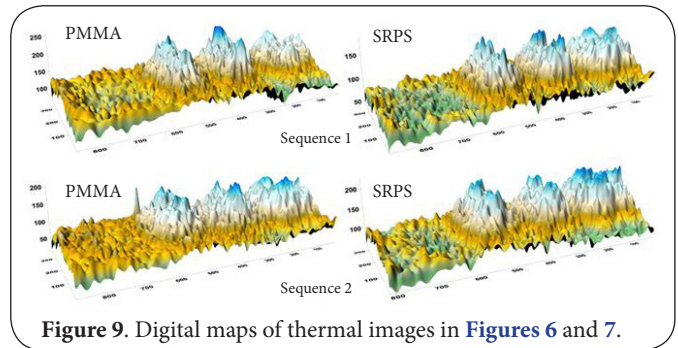
**Figure 9**. Digital maps of thermal images in **Figures 6** and **7**.

With the digital map available, it is possible to compute basic parameters of non-uniformity. The most important is maximum variation, i.e. how big the swing of temperature is. For that, the absolute maximumv T_{max} and T_{min} must be computed, and the swing is T_{max}-T_{min}. Sometimes, this parameter is called «peak-to-valley» value. However, this value shows only local maximum variation and does not tell how often such a big variation occurs in the entire phantom. Therefore, the variation averaged over the phantom area may be useful, which is characterized by real mean square variation RMS:

$$\text{RMS} = \sqrt{\frac{1}{\sigma} \int \left[\text{T}(\vec{r}) - \text{T}_{\text{average}} \right]^2 d^2 r} \; , \qquad (2)$$

which requires computation of the average temperature over the entire area σ :

$$\text{T}_{\text{average}} = \frac{1}{\sigma} \int \text{T}(\vec{r}) d^2 r \qquad (3)$$

Another parameter that may be of interest is the area S within which the temperature exceeds the value T - cumulative area distribution. This parameter is a function of T, and is better presented by the dimensionless ratio $S(T)/\sigma$ (**Figure 10**). It characterizes simultaneously uniformity (the sharper the slope the better uniformity) and maximum variation (the length of the slope is maximum variation of temperature). Also, it may be interesting what part of the phantom area p is in the temperature interval between T and T+dT - the probability of finding the temperature T in the phantom. Commonly, dT - the minimum detectable temperature difference–is equal to 0.1°C. This distribution is shown in **Figure 11**. The maximum of this distribution is at T_{mp} –most probable temperature within a phantom. **Table 1** summarizes these data.
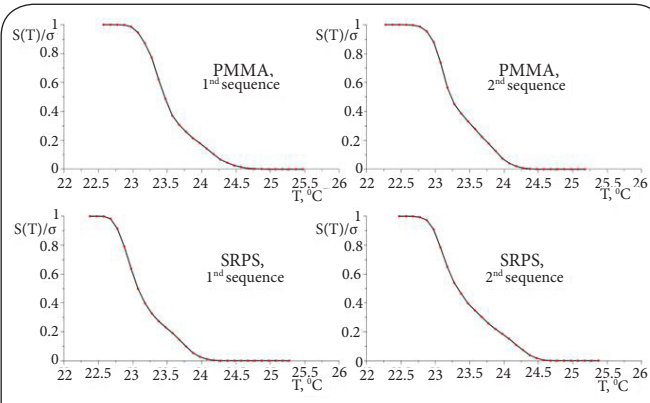
Figure 10. Cumulative area distribution for PMMA (upper row) and SRPS (lower row) phantoms after 1st (at left) and 2nd (at right) sequences.
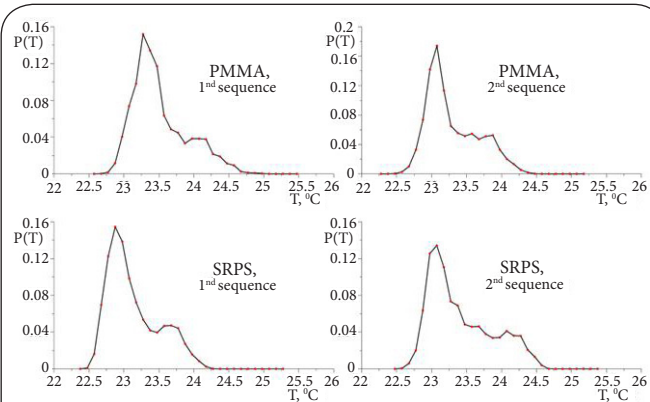
Figure 11. Probability of finding temperature in PMMA (upper row) and SRPS (lower row) phantoms after 1st (at left) and 2nd (at right) sequences.

Table 1. Temperatures of the phantoms before and after exposure (Centigrade).

Phantom	Sequence	T_{max}	T_{min}	$T_{max}-T_{min}$	$T_{average}$	T_{mp}	RMS
PMMA	1	25.0	22.7	3.0	23.6	23.3	0.39
	2	24.5	22.4	2.1	23.4	23.1	0.37
SRPS	1	24.3	22.5	1.8	23.2	22.9	0.36
	2	24.7	22.6	2.1	23.5	23.1	0.46

Thus, extensive mathematical treatment of the IR images formed by large numerical arrays of the size of hundreds of pixels provides much more comprehensive information than can be expected from any technique based on discrete sensors.

Conclusions

For validation of uniformity of radio-frequency (RF) coils in MRI scanners, thermo-vision cameras offer great flexibility, non-invasiveness, high temperature precision, and excellent spatial resolution.

This technology, combined with specially designed phantoms, digital representation of the temperature maps,

and extensive mathematical treatment of the results, offers new possibilities, inaccessible for traditional methods based on discrete sensors.

Thin solid-state dielectric phantoms opaque in IR optical domain, with small thermal conductivity, are inexpensive and easy to manufacture tools for measuring spatial non-uniformity. Unlike volumetric liquid or gelatinous phantoms, they are insensitive to stirring and unambiguous in a sense that the result is not influenced by the walls, IR transparency, or thermal diffusion in liquid. As another advantage, they may be positioned either vertically or horizontally.

Competing interests
The author declares that he has no competing interests.

References

1. Collins CM. **RF Safety and Guidelines: Simulations in MRI. ESMRMB Lectures on RF Simulation for MR Systems: Coil Design and Safety, Utrecht**. Netherlands. 2013; 12-14.

2. Frohlich J. **Numerical Methods in RF Coil Design**. **ESMRMB Lectures on RF Simulation for MR Systems: Coil Design and Safety, Utrecht**. Netherlands. 2013; 12-14.

3. Kraff O. **Validation Methods**. **ESMRMB Lectures on RF Simulation for MR Systems: Coil Design and Safety, Utrecht**. Netherlands. 2013; 12-14.

4. Sommer T, Vahlhaus C, Lauck G, von Smekal A, Reinke M, Hofer U, Block W, Traber F, Schneider C, Gieseke J, Jung W and Schild H. **MR imaging and cardiac pacemakers: in-vitro evaluation and in-vivo studies in 51 patients at 0.5 T**. *Radiology*. 2000; **215**:869-79. | Article | PubMed

5. Graesslin I, Glaesel D, Biederer S, Schwesser F, Vernickel P, Baornet P, Annighoefer B, Stahl H, Dingemans H, Mens G, Harvey P and Katscher U. **SAR in Parallel Transmission**. *PIERS Online*. 2008; **4**:681-685. | Article